# Minnaert resonance in an array of two-dimensional bubbles

Camila Horvath,[1,*] Yolanda Vargas-Hernández,[2] and María Luisa Cordero[1]

[1]*Departamento de Física, FCFM, Universidad de Chile, Av. Blanco Encalada 2008, Santiago, Chile*
[2]*Departamento de Física, Universidad de Santiago de Chile, Av. Víctor Jara 3493, Santiago, Chile*

Transmission and reflection of sound across a dense layer of long rectangular quasi-two-dimensional bubbles in a polymeric matrix are measured over two frequency ranges, 150–260 and 670–1130 kHz. Contrary to what is expected, considering the high acoustic impedance contrast between air and the matrix, there is high transmission across the layer, especially in the lower-frequency range. These results are explained by a monopolar Minnaert-like resonance of bubbles, which radiates sound in both directions of the bubble layer. The Minnaert resonance is computed for two-dimensional bubbles, revealing a resonance frequency within the lowest-frequency range used. The transmission and reflection coefficients are theoretically computed by considering the bubble array as a homogeneous layer with a resonant acoustic impedance.

## I. INTRODUCTION

Due to their high compressibility, air bubbles in a liquid medium are monumentally efficient sound scatterers. For this reason, air bubbles contained in a fluid medium can dramatically affect the values of sound velocity and acoustic attenuation, even for very low gas fractions [1]. These properties make bubbles relatively easy to identify, making acoustic measurements an important and nondestructive tool to characterize the presence of bubbles in different media, such as dough [2] or the sea [3], and bubbles are excellent contrast agents in ultrasound measurements [4].

Resonant scattering for a bubbly medium can happen over a very wide frequency range, resulting, for example, in multiple band gaps for acoustic waves related to the existence of multiple Mie resonances in bubble metacrystals [5], which even survive positional disorder [6,7]. One of the most prominent features of bubbles is their lowest-frequency resonance, usually known as the Minnaert resonance [8]. The Minnaert resonance causes bubbles to radially oscillate in response to the incident pressure wave, which typically occurs for wavelengths much larger than the bubble size. As a reference, a 1-mm-radius bubble in water has a Minnaert resonance at a frequency of around 3 kHz, which corresponds to a wavelength of, approximately, 0.5 m.

Interestingly, the Minnaert resonance is maintained when bubbles are trapped in a yield-stress fluid [9,10] or even a soft elastomer [11]. Treatment of air-filled spherical cavities embedded in an elastic matrix can be found,

for example, in Refs. [12–14]. As long as the shear modulus of the elastic medium is low enough, the low-frequency response of the bubble, characteristic of the Minnaert resonance, remains. Since trapping and localization of bubbles in soft elastomers are possible, the intelligent design of bubble-based acoustic metamaterials is feasible. For example, ordered arrays of bubbles have been proposed and used for the fabrication of two- and three-dimensional metacrystals, exhibiting a band gap associated with the resonant nature of the bubbles [15,16]. Another example consists of the development of superabsorptive metascreens, which are demonstrated with a very thin polymeric layer containing an array of encapsulated bubbles, that decrease not only sound transmission [17] but also its reflection [18]. Also, almost perfect absorption of two counterpropagating sound waves, a phenomenon known as coherent perfect absorption, is demonstrated in a similar setup by carefully designing the bubble size and spacing [19]. These results are important for soundproofing and the development of acoustic cloaking covers.

Many of the examples presented above use short cylindrical cavities, the characteristic sizes of which are in the range of 10–100 $\mu$m and that are replicated in polymers from molds made by optical lithography. However, for practical applications, long cavities resembling quasi-two-dimensional bubbles might be simpler to replicate in polymers from molds fabricated through more affordable manufacturing methods, such as 3D printing or micromachining. Accordingly, a description of the Minnaert-like resonance of two-dimensional bubbles is of interest. Despite knowing the resonant behavior of spherical bubbles for almost a century, its extension to two-dimensional

*camila.horvath@ing.uchile.cl

bubbles has scarcely been studied. The main problem is that direct application of Minnaert's argument for calculation of the resonance frequency in two dimensions leads to a logarithmic divergence of the kinetic energy associated with the velocity field outside the radially oscillating bubble. In other words, the effective mass of this harmonic resonator diverges in the two-dimensional case [20]. Although the frequency of the Minnaert resonance for a two-dimensional bubble was studied by Ammari *et al.* in terms of a transcendental equation [21], no experimental confirmation of this phenomenon has been reported so far.

Here, we study sound propagation across a thin layer of very long cavities of rectangular cross section embedded in a polymeric matrix. In practice, the cavities can be considered as two-dimensional rectangular bubbles. When forced by a sound wave, we measure an important transmission and reflection across the bubble layer, and we argue that this behavior can be tracked to a Minnaert-like resonance of the two-dimensional bubbles. These results might be important for the future development of bubble-based metamaterials.

## II. EXPERIMENTAL METHODS

### A. Fabrication of the array of two-dimensional bubbles

A periodical array of long rectangular air inclusions was fabricated in a polydimethylsiloxane (PDMS) matrix. The acoustic properties of PDMS are similar to those of water [22–25]. In particular, we measure a sound speed of $c_{\text{PDMS}} = 1046$ m/s for PDMS using two transducers, an arbitrary waveform generator (Agilent) and an oscilloscope (TiePieSCOPE HS805), sending an echo pulse of frequency 1 MHz. The PDMS density is $\rho_{\text{PDMS}} = 920$ kg/m$^3$.

The array of bubbles was fabricated using standard lithography and soft lithography techniques [26]. First, a negative mold was patterned through optical lithography in SU-8 on top of a 150-mm-diameter silicon wafer using a maskless laser writer (Heidelberg MLA100). PDMS and the curing agent (Sylgard 184, Dow Corning) were mixed in a 10:1 ratio (in weight) and degassed for 45 min over the counter. The mold was coated with a thin layer of PDMS using a spin coater at 500 rpm, and then baked for 40 min at 65 °C in a convection oven to obtain a partially cured but manipulable texturized film. In the same way, a thin PDMS layer was obtained by spin coating a flat silicon wafer, which was baked for 20 min. The texturized PDMS film was peeled off the mold and placed against the flat PDMS thin film. The whole material was baked for 8 h at 65 °C in a convection oven to irreversibly bond both surfaces, resulting in a periodical array of air bubbles inside a thin film of PDMS. Cavities are naturally filled with air during the fabrication process. The curing process of PDMS does not produce any gaseous byproduct, but, in
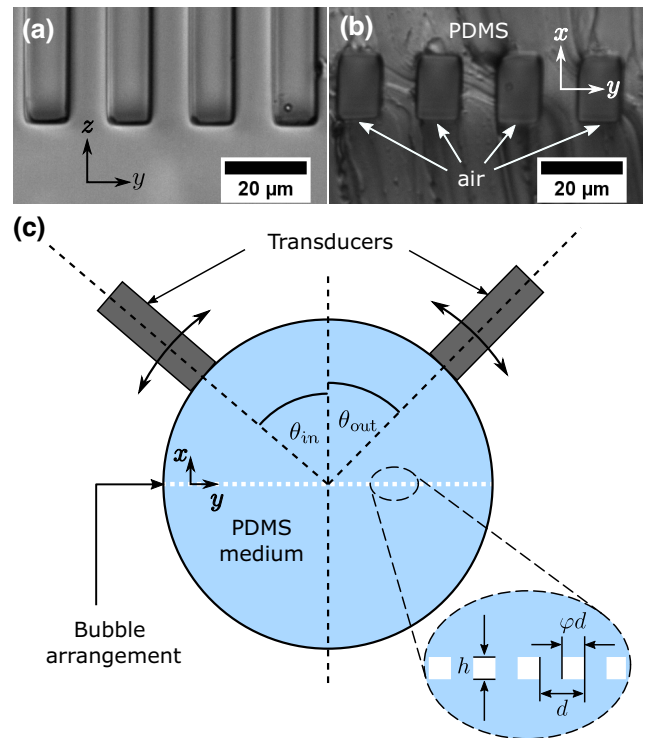


FIG. 1. (a),(b) Top and front views, respectively, of the periodical array of rectangular air bubbles on a PDMS matrix. (c) Schematic of the experimental setup used to measure the acoustic response of the bubble array.

the event of that happening, gas contamination will eventually dissipate through PDMS, which is permeable to gases. Also, residual stresses are avoided as far as possible during assembly, and they are expected to relax during the final bake. Thanks to the photoelastic nature of PDMS, residual stresses can be revealed by illuminating the sample with polarized light and observing through a perpendicular polarizer. Inspection of the bubble array in this way did not show any residual stresses.

The resulting array has a periodicity of $d = 20$ μm, void fraction of $\varphi = 0.5$, and height of $h = 18$ μm [Fig. 1(c)], where each of the air cavities, with a width of $\varphi d = 10$ μm, has an extension of 90 mm along the $z$ axis. The overall bubble array spans a square with 90-mm sides, and the thickness of the resulting PDMS layer containing the bubble array is approximately 0.6 mm. Pictures of top and lateral views of the assembled array are displayed in Figs. 1(a) and 1(b), respectively. The lateral view of the structure is obtained by cutting a thin slice perpendicular to the array. The pictures were acquired using a camera mounted to a microscope and placing the samples on a microscope slide.

### B. Experimental setup

The PDMS layer with the bubble array was placed between two PDMS semicylinders, as shown in Fig. 1(c).

The sealing between the PDMS semicylinders and the layer with bubbles was reversible, taking advantage of the conformal PDMS-PDMS adherence that produces stable full contact between the surfaces [26].

To measure the transmission across a homogeneous air layer, two 5-mm-wide 37-μm-thick paper strips were used as spacers between the two semicylinders by placing them at opposite extremes of the gap.

The whole PDMS cylinder, with a diameter of $D = 94$ mm and length of 105 mm, was placed on a home-made acrylic setup that also held two acoustic transducers around the cylinder, pointing to its center [Fig. 1(c)]. Two pairs of transducers were used to work at two different frequency ranges. The first one was a pair of homemade transducers that worked in the range 150–260 kHz (TP1), and the second pair (Olympus V303) worked between 670 and 1130 kHz (TP2). Couplant gel (Olympus D12) was used between the transducers and the surface of the cylinder. One of the transducers acted as an emitter and was excited with a continuous sinusoidal signal of frequency $f$. The other transducer acted as a receiver to measure the reflected and transmitted acoustic signals.

The emitting and receiving transducers were placed at angles of $\theta_{in}$ and $\theta_{out}$ with respect to the normal to the bubble array, $x$ (see Fig. 1). The position of the two transducers was controlled independently in $5°$ steps. The measurements were performed by varying the position of both transducers and gradually changing the frequency of the incident wave.

A signal generator (Rigol DG1022), set with a continuous sinusoidal signal of constant amplitude, was used to excite the emitter transducer, and the response was measured by changing the signal frequency in steps of 0.1 kHz. In the case of TP1, the emitter was directly connected to the signal generator, and the sinusoidal signal was set at
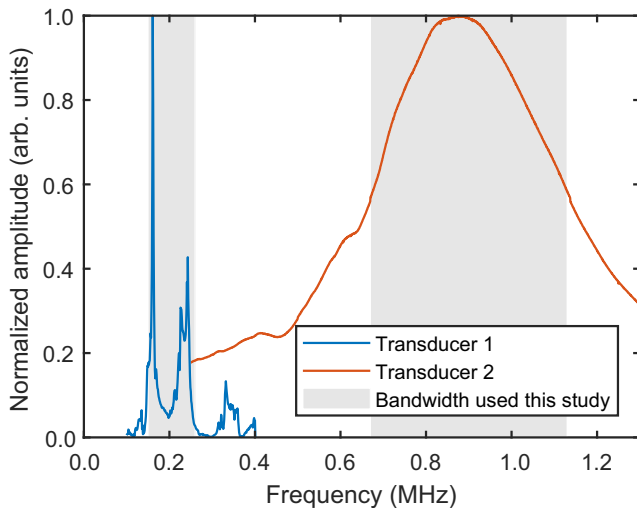
7 $V_{pp}$. In the case of TP2, 2 $V_{pp}$ was amplified 20 times by a high-speed bipolar amplifier (HSA 4011) placed between the signal generator and the emitter transducer. The receiving transducer was directly connected to an oscilloscope (Tektronix TBS1102B) to analyze the acoustic signal.

The frequency response of the transducers was measured with the two transducers in direct contact through the couplant gel and using a continuous sinusoidal signal for the excitation. These normalized responses are shown in Fig. 2.

Note that for the two frequency ranges used in this study, the wavelength is always larger than the characteristic size of the bubbles. In PDMS, the wavelengths range between 4 and 7 mm for TP1 and between 0.9 and 1.6 mm for TP2. In air, the wavelengths range between 1.3 and 2.3 mm for TP1 and between 0.3 and 0.5 mm for TP2.

## III. RESULTS

### A. Background

First, the acoustic response of the PDMS cylinder without the bubble layer was characterized to establish a background to compare the response of the bubble array. For each pair of transducers, we measure the beam profile, which is the intensity of the acoustic signal measured by the receptor transducer along the surface of the cylinder for a fixed position of the emitter transducer. Figures 3(a) and 3(b) show the normalized beam profiles measured in the solid cylinder as a function of $\theta_{out}$ and $f$ for fixed $\theta_{in} = 10°$ for TP1 and $\theta_{in} = 0°$ for TP2. The beam profiles were normalized by the corresponding frequency response of the transducers shown in Fig. 2. Also, the signal was corrected for attenuation in PDMS by dividing the received signal by $e^{-\alpha D}$, where $\alpha = 0.023f^{1.54}$ mm$^{-1}$, with $f$ in MHz, is the attenuation coefficient for sound in PDMS, as obtained from Ref. [27]. As shown in Fig. 3(a), the beam profile for TP1 is quite wide. Nevertheless, as shown by dashed lines in Fig. 3, a marked maximum is observed around $\theta_{out} = 180° - \theta_{in} = 170°$, which accounts for transmission of the acoustic wave across the solid PDMS cylinder. As expected, no reflections were measured at $\theta_{out} = \theta_{in}$, proving that the quality of conformal contact between the PDMS surfaces was good. Figure 3(b) exhibits a more focused beam profile for TP2, showing a maximum at the exact opposite of the incident angle, $\theta_{out} = 180°$.

### B. Transmission and reflection coefficients at low frequencies

Next, we study the interaction between a sinusoidal acoustic wave and the layer of air bubbles for frequencies between 150 and 260 kHz with TP1. The transmitted and reflected signals were measured as a function of the incident angle, $\theta_{in}$, by placing the receiving transducer at angles of $\theta_{out} = 180° - \theta_{in}$ and $\theta_{out} = \theta_{in}$. The measured



FIG. 2. Frequency response of transducers normalized by their maximum value.

**(a)**



**(b)**
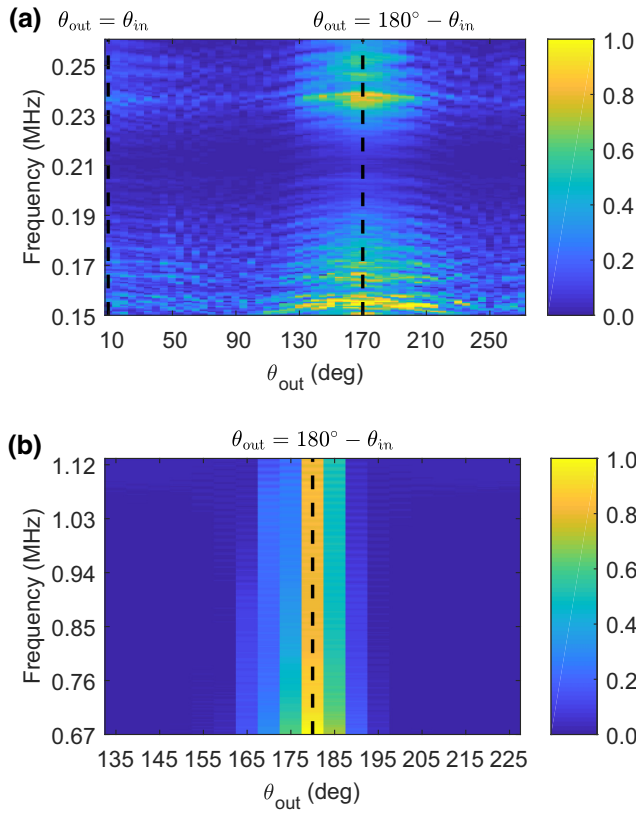


FIG. 3. (a) Beam profile measured with TP1 for incident angle $\theta_{\text{in}} = 10°$. (b) Beam profile measured with TP2 for normal incidence, $\theta_{\text{in}} = 0°$. Black dashed lines mark the angles for the expected transmitted and reflected acoustic beams, which would be at angles $\theta_{\text{out}} = 180° - \theta_{\text{in}}$ for the transmitted wave and $\theta_{\text{out}} = \theta_{\text{in}}$ for the reflected wave.

**(a)** $|T|$

**(b)** $|R|$

**(c)** $\sqrt{|T|^2 + |R|^2}$



FIG. 4. (a) Transmission coefficient $|T|$, (b) reflection coefficient $|R|$, and (c) $\sqrt{|R|^2 + |T|^2}$ as a function of frequency and incidence angle.

signals, corrected by the frequency response of the transducers (Fig. 2) and by sound attenuation in PDMS, were normalized by the background signal at $\theta_{\text{out}} = 180° - \theta_{\text{in}}$ for transmission and at $\theta_{\text{out}} = \theta_{\text{in}}$ for reflection.

Figure 4 shows the resulting transmission and reflection coefficients, $|T|$ and $|R|$, as well as $\sqrt{|T|^2 + |R|^2}$, as a function of both frequency and incident angle. In general, for $\theta_{\text{in}} > 55°$, little acoustic signal is transmitted across the bubble layer and most is reflected. Conversely, for $\theta_{\text{in}} < 55°$, transmission is important. Overall, the total intensity, $|T|^2 + |R|^2$, remains roughly constant, except for a very oblique incidence of $\theta_{\text{in}} = 85°$, when most of the acoustic signal is absorbed over the whole frequency range.

A frequency modulation in both $|T|$ and $|R|$ is observed. This modulation might be caused by internal resonances of the semicylinders, since this modulation is also present in the background of Fig. 3(a).

To put these results into context, we performed similar measurements with the bubble array replaced by a thin homogeneous air layer. In this case, the transmission coefficient is much lower than the reflection coefficient, and
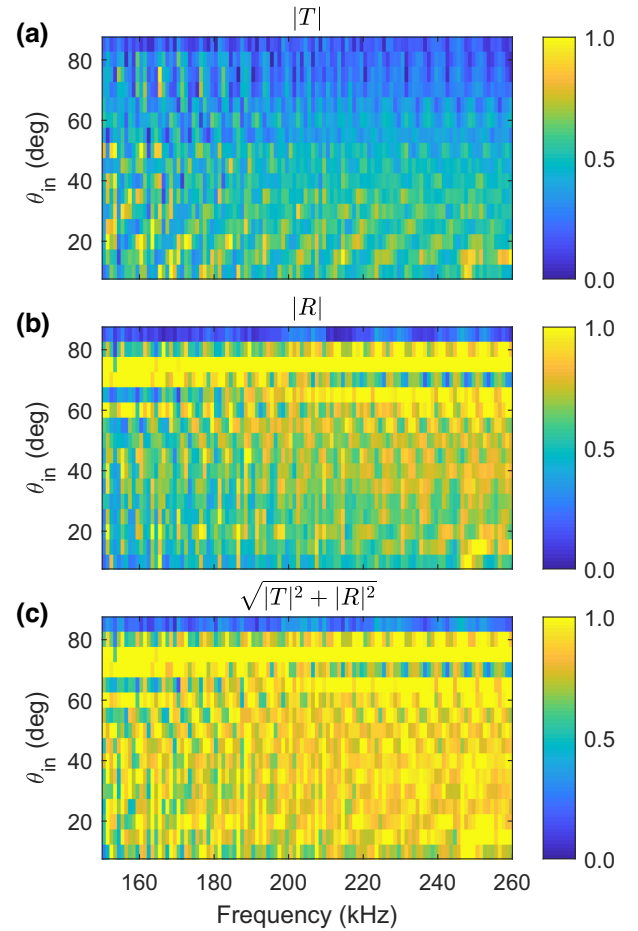
most of the acoustic signal is reflected, for all incidence angles. As an example, the transmission and reflection coefficients measured for $\theta_{\text{in}} = 20°$ across the homogeneous air layer ($T_{\text{air}}$ and $R_{\text{air}}$) are shown in Fig. 5(a). These results can be contrasted with the classic result of transmission and reflection of an acoustic wave across a homogeneous layer of thickness $h$ [28], as presented in Appendix A. Accordingly, the theoretical reflection and transmission coefficients across an air layer for oblique incidence, Eqs. (A4) and (A5), are shown in Fig. 5(a) ($T_{\text{theo}}$ and $R_{\text{theo}}$). The thickness of the layer was varied between 18 μm (the thickness of the bubble layer) and 37 μm (the measured thickness of the air layer). One can observe that reflection and transmission across the homogeneous air layer is reasonably well described by the classical theory of reflection and transmission across a layer of different specific acoustic impedance than the outer medium, and that the transmission coefficient in this case is 3 orders of magnitude lower than the reflection coefficient. However, the agreement is not quantitative, since theory predicts an
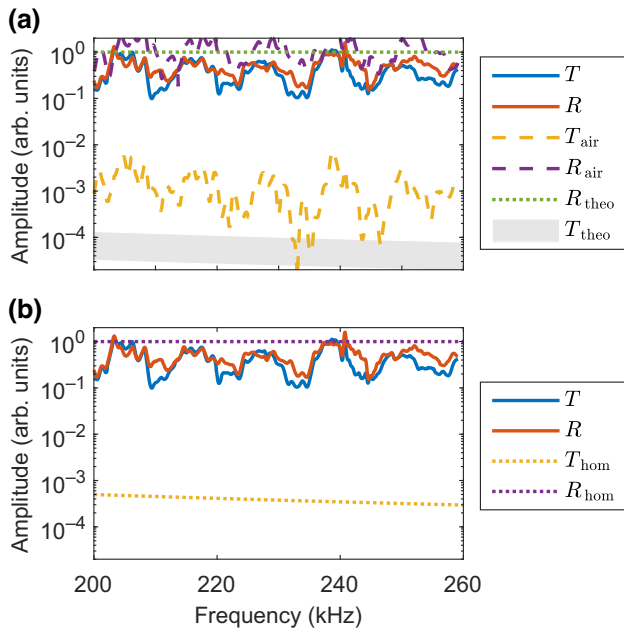
FIG. 5. (a) Experimental transmission and reflection coefficients in the bubble array ($T$, $R$), and in a 37-µm-thick homogeneous air layer ($T_{air}$, $R_{air}$). Theoretical transmission and reflection coefficients for an incident wave across the homogeneous air layer are shown as $T_{theo}$ and $R_{theo}$. $T_{theo}$ is a band representing the theoretical results for an air layer of thickness between 18 and 37 µm. (b) Same experimental measurements in the bubble array ($T$, $R$) are compared with theoretical results of transmission and reflection through an effective medium of 18 µm thick ($T_{hom}$ and $R_{hom}$).

even lower transmission. The difference might be due to the resonances of the whole cylinder causing frequency modulations, also observed here, but this could also be due to a poor signal-to-noise ratio when the acoustic signal is low.

The low transmission across the homogeneous air layer can be well explained by the high acoustic impedance contrast between air and PDMS, as explained in Appendix A. Therefore, it seems surprising that the bubble layer, which has a similar thickness to the air layer and is formed by 50% air, has a much larger transmission coefficient. The transmission and reflection coefficients for the same $\theta_{in} = 20°$ across the bubble layer ($T$ and $R$) are shown in Fig. 5(a). In this case, the transmission and reflection coefficients across the bubble array are comparable to each other in magnitude, with the transmission coefficient being much larger than expected for an 18-µm-thick air layer.

The same theoretical calculation can be used to predict the transmission and reflection coefficients for the bubble layer but using a homogenization method to consider the bubble layer as an effective medium [29–31], thus taking into account the spatially varying acoustic properties within the bubble layer. The transmission and reflection

coefficients through the effective medium that replaces the bubble layer obtained from this method are presented in Appendix B, see Eqs. (B6) and (B7). It is clear from Fig. 5(b) that this approach is not adequate. Here, the same experimental transmission and reflection coefficients obtained with $\theta_{in} = 20°$ ($T$ and $R$) are compared to the theoretical results obtained for the reflection and transmission coefficients through the effective medium for an oblique incident wave at $\theta_{in} = 20°$ ($T_{hom}$ and $R_{hom}$). The transmission predicted by the homogenization method is much lower than the measured transmission across the bubble layer. In fact, for our geometrical parameters, the homogenization method yields an effective medium with an acoustic impedance approximately twice the acoustic impedance of air, which is still much lower than the acoustic impedance of PDMS. Thus, the homogenization method predicts very low transmission through the effective medium, and an alternative explanation should be considered.

## C. Transmission and reflection coefficients at high frequencies

Similar measurements were performed using TP2. The results are shown in Fig. 6. In this higher-frequency range, the transmission coefficient is significantly lower than the reflection coefficient.

Figure 7 compares the experimental results for an incident angle of $\theta_{in} = 20°$ with the results of homogenization theory ($T_{hom}$, $R_{hom}$). Again, there is poor agreement between the theoretical predictions for the transmission
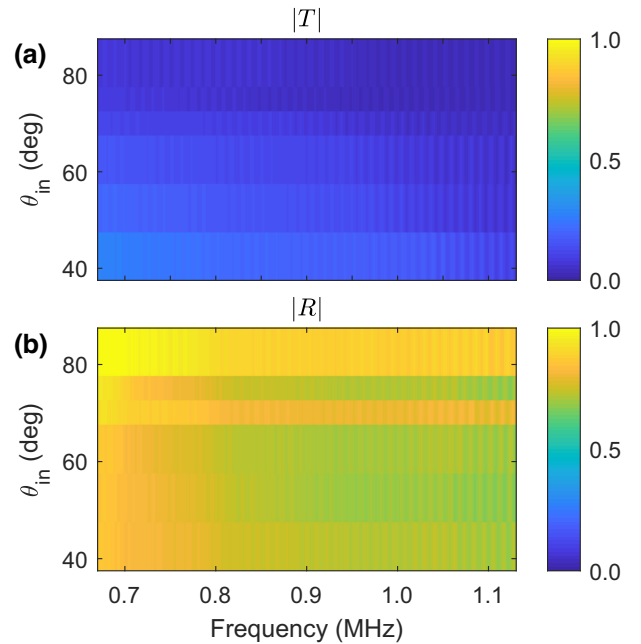


FIG. 6. (a) Transmission and (b) reflection coefficients in the bubble array measured using TP2.
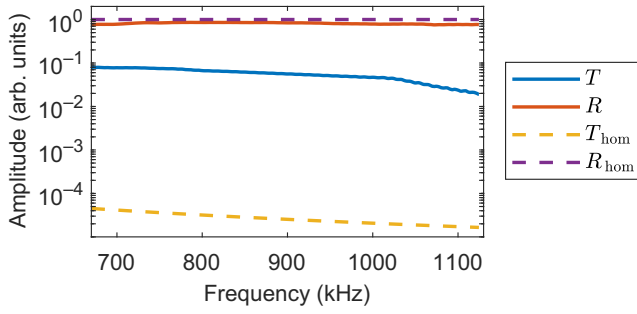
FIG. 7. Transmission and reflection coefficients in the bubble array ($T$, $R$) and those obtained using homogenization theory ($T_{\mathrm{hom}}$, $R_{\mathrm{hom}}$).

coefficient and the measured one, with experimental data showing a much higher transmission than that predicted by the theoretical results. However, in comparison with data obtained at lower frequencies, the transmission coefficient is 1 order of magnitude lower than the reflection coefficient.

## IV. MODEL

### A. Minnaert resonance in two dimensions

Our results confirm that the bubbles cannot be considered as simple scatterers of the acoustic wave. This is to be expected, since gas bubbles are well known for their high scattering efficiency, which mostly comes from low-frequency resonances, such as the Minnaert resonance. Therefore, we propose here that the origin of high transmission at low frequency is a Minnaert-like resonance of the two-dimensional bubbles and determine its frequency. Our derivation is based on the work by Devaud *et al.* for the resonance of a three-dimensional bubble [32], which determines the bubble radial oscillations in response to an incident sound field and computes the accompanying scattered sound field due to these oscillations.

Consider a circular gas bubble in a two-dimensional infinite medium. Suppose that an external acoustic wave is incident on the bubble, causing it to radially pulsate around an equilibrium radius, $R_0$. This oscillation will, in turn, produce a scattered acoustic wave in the outer medium and a pressure wave inside the bubble. The acoustic pressure, both outside and inside the bubble, satisfies the Helmholtz equation:

$$\nabla^2 p_j + k_j^2 p_j = 0, \tag{1}$$

where the subindex $j = \mathrm{out}$ indicates quantities outside the bubble and $j = \mathrm{int}$ is for those inside the bubble. A dependence in time of the form $e^{-i\omega t}$ is assumed, such that $k_j = \omega/c_j$, where $c_j$ is the sound speed in each medium. The displacement field both inside and outside the bubble

can be computed from the pressure fields as

$$\vec{u}_j(r) = \frac{1}{\rho_j \omega^2} \nabla p_j, \tag{2}$$

where $\rho_j$ denotes the density of each medium.

Using polar coordinates $(r, \theta)$ centered in the bubble, and focusing on the monopolar response of the bubble, the solution of Eq. (1) for $p$ is a combination of Bessel functions of the first and second kind and zero order, $J_0(k_j r)$ and $Y_0(k_j r)$. Regularity of the solution inside the bubble requires, for $r \leq R$,

$$p_{\mathrm{int}} = A J_0(k_{\mathrm{int}} r), \tag{3}$$

$$u_{\mathrm{int}} = -\frac{A k_{\mathrm{int}}}{\rho_{\mathrm{int}} \omega^2} J_1(k_{\mathrm{int}} r), \tag{4}$$

where $A$ is the pressure amplitude of the inner wave. Outside the bubble, a more suitable solution for $p$ is written in terms of Hankel functions of first and second kind and zero order, which yields

$$p_{\mathrm{out}} = W_{\mathrm{sc}} H_0^{(1)}(k_{\mathrm{out}} r) + W_{\mathrm{in}} H_0^{(2)}(k_{\mathrm{out}} r), \tag{5}$$

$$u_{\mathrm{out}} = -\frac{k_{\mathrm{out}}}{\rho_{\mathrm{out}} \omega^2} \left( W_{\mathrm{sc}} H_1^{(1)}(k_{\mathrm{out}} r) + W_{\mathrm{in}} H_1^{(2)}(k_{\mathrm{out}} r) \right), \tag{6}$$

for $r \geq R$. These expressions are useful as the first terms on the right-hand sides represent an outgoing (to $r \to \infty$) radially symmetric wave, while the second terms represent an incoming (to $r = 0$) radially symmetric wave. Accordingly, $W_{\mathrm{in}}$ corresponds to the pressure amplitude of the monopolar contribution to the incident wave and is considered to be given, while $W_{\mathrm{sc}}$ corresponds to the amplitude of the pressure wave associated with radial oscillations of the bubble.

Continuity of pressure and displacement at $r = R_0$ yield the pressure amplitudes of the scattered and internal waves, both normalized by the amplitude of the incident pressure field:

$$\frac{A}{W_{\mathrm{in}}} = q \frac{-H_1^{(1)}(\alpha x_{\mathrm{int}}) H_0^{(2)}(\alpha x_{\mathrm{int}}) + H_0^{(1)}(\alpha x_{\mathrm{int}}) H_1^{(2)}(\alpha x_{\mathrm{int}})}{J_1(x_{\mathrm{int}}) H_0^{(1)}(\alpha x_{\mathrm{int}}) - q J_0(x_{\mathrm{int}}) H_1^{(1)}(\alpha x_{\mathrm{int}})}, \tag{7}$$

$$\frac{W_{\mathrm{sc}}}{W_{\mathrm{in}}} = \frac{-J_1(x_{\mathrm{int}}) H_0^{(2)}(\alpha x_{\mathrm{int}}) + q J_0(x_{\mathrm{int}}) H_1^{(2)}(\alpha x_{\mathrm{int}})}{J_1(x_{\mathrm{int}}) H_0^{(1)}(\alpha x_{\mathrm{int}}) - q J_0(x_{\mathrm{int}}) H_1^{(1)}(\alpha x_{\mathrm{int}})}. \tag{8}$$

In these expressions, we defined $x_{\mathrm{int}} = k_{\mathrm{int}} R_0$, and the contrasts of sound velocity and acoustic impedance between the internal and the external medium, $\alpha = c_{\mathrm{int}}/c_{\mathrm{out}}$ and $q = \rho_{\mathrm{int}} c_{\mathrm{int}}/\rho_{\mathrm{out}} c_{\mathrm{out}}$, respectively.

At this point, one notices that an internal and a scattered wave exist for any frequency of the incident wave, and therefore, there are no resonances in the strict sense
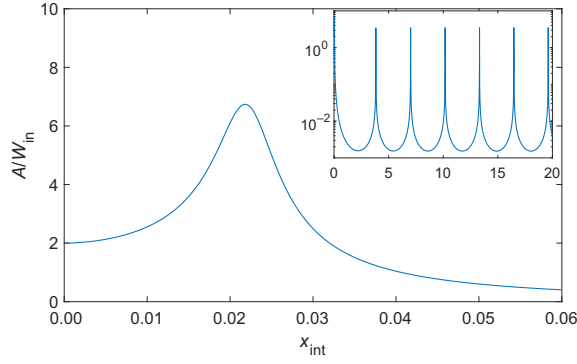
FIG. 8. Normalized pressure amplitude inside the bubble as a function of $x_{int}$, which is computed from Eq. (7) with air and PDMS values of sound velocity and acoustic impedance. Inset shows several peaks for a wide range of $x_{int}$, while the main figure shows a magnification of the first peak.

of the term. However, one can look for situations where the inner pressure amplitude is maximized; this was previously related to resonancelike behavior [32]. The inset in Fig. 8 shows the normalized pressure amplitude inside an air bubble in PDMS, which presents a series of maxima. Most of these maxima are associated with small wavelengths ($x_{int} > 1$), where the monopolar approximation for the bubble response is inadequate. However, the first one is a low-frequency peak, at $x^*_{int} \approx 0.0218 \ll 1$, see Fig. 8. The corresponding resonance frequency is thus given by $f_0 = c_{int} x^*_{int}/(2\pi R_0)$.

For a bubble of radius $R_0^{eq} = 7.6$ μm (that is, a circular bubble with the same area as the rectangular bubbles of the experiment), this corresponds to a frequency of $f_0^{th} = 157$ kHz. In comparison, the Minnaert frequency for a spherical bubble of the same radius is approximately 450 kHz, almost 3 times larger.

### B. Resonant layer

The resonant nature of the bubbles allows us to understand the system of a single two-dimensional bubble as being a standard resonator with natural (angular) frequency $\omega_0 = 2\pi f_0$, just as in the three-dimensional case of the Minnaert resonance [33–35]. The scattering function for this resonant system is

$$F_s = \frac{R_0}{(\omega_0/\omega)^2 - 1},$$ (9)

such that, given an plane incident pressure wave traveling in the $x$ direction, $p_0 e^{i(kx-\omega t)}$, the radially symmetric radiated pressure wave will be described as $F_s/r\, p_0 e^{i(kr-\omega t)}$ [10]. If we now consider the bubble layer, formed by $N$ such resonant bubbles per unit volume, then Foldy's law [36] states that the wave number in the layer will be
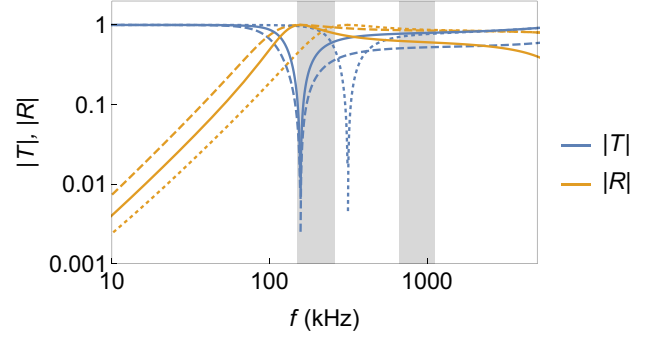


FIG. 9. Predicted transmission and reflection coefficients for oblique incidence across a layer composed of resonant bubbles. For evaluation, the following values were used: $f_0 = 157$ kHz and $R_0 = 7.6$ μm (solid lines); $f_0 = 157$ kHz and $R_0 = 15.2$ μm (dashed lines); $f_0 = 314$ kHz and $R_0 = 7.6$ μm (dotted lines). Gray regions mark the frequency ranges studied in the experiment.

given by

$$k_{layer}^2 = k_{out}^2 + 4\pi N F_s.$$ (10)

Foldy's prediction amounts, in our case, to having a layer with a resonant specific acoustic impedance, $Z_{layer} = \rho_{layer} c_{layer}$, with $c_{layer} = \omega/k_{layer}$. Therefore, one can compute the transmission and reflection coefficients by using the classical theory for oblique incidence of an acoustic wave at a homogeneous layer, Eqs. (A4) and (A5). The results are plotted in Fig. 9. For the evaluation, an average mass density for the layer $\rho_{PDMS}/2$ was considered, because the void fraction of our bubble layer was $\varphi = 0.5$ and the air density was negligible in comparison with the PDMS one. The number of bubbles per unit volume is estimated as

$$N = \frac{\lambda_{out}/d}{h\lambda_{out}^2} = \frac{k_{out}}{2\pi h d},$$ (11)

i.e., the number of bubbles that fit within a volume given by a parallelepiped of square base of length equal to the wavelength, $\lambda_{out} = 2\pi/k_{out}$, and height equal to the bubble-layer thickness, $h$.

A quantitative comparison between the model and experiments is difficult, since several approximations are in place, see Sec. V. However, the results presented in Fig. 9 for transmission and reflection across the resonant layer, in contrast with the results of transmission and reflection across a homogeneous air layer, and across an effective homogenized layer, predict high transmission at low frequencies, $f \ll f_0$, and at high frequencies, $f \gg f_0$. A minimum of transmission, coinciding with a maximum of reflection, is predicted at the resonant frequency, $f_0$. This minimum was not observed in our measurements, which would indicate that the exact values of $f_0$ and $R_0$ were not the ones found above.

The effect of varying $f_0$ and $R_0$ is shown in Fig. 9. The solid line is computed with $f_0 = f_0^{\text{th}}$ and $R_0 = R_0^{\text{eq}}$, the dashed line with $f_0 = 2f_0^{\text{th}}$ and $R_0 = R_0^{\text{eq}}$, and finally the dotted line is for $f_0 = f_0^{\text{th}}$ and radius $R_0 = 2R_0^{\text{eq}}$. One can confirm that the location of the transmission minimum follows the position of $f_0$. On the other hand, increasing $R_0$ causes, in general, an overall decrease in $T$ and an increase in $R$. Based on this, it seems possible to find appropriate values of $f_0$ and $R_0$ to obtain transmission and reflection coefficients of similar magnitude in the first frequency range explored in the experiment, just as in our measurements. Conversely, it appears that, in the second frequency range, $|T|$ is predicted to be larger than $|R|$, in contradiction to the experiments. However, at larger frequencies, the monopolar response of the bubbles assumed here becomes a progressively worse approximation. A dipolar response of the bubbles to the incident sound wave could play a relevant role in explaining the acoustic response of the bubble layer in the higher-frequency range studied here [37].

## V. DISCUSSION

For a thin layer of two-dimensional bubbles, such as the one studied in the present work, a calculation based on homogenization predicts low transmission and high reflection. Our experimental results reveal that it is a poor prediction, with the layer being as transmissive as it is reflective in the lowest-frequency range used, between 150 and 260 kHz. At the higher-frequency range used in this study, between 670 and 1130 kHz, the layer is significantly more reflective than transmissive, with the transmission coefficient being approximately 1 order of magnitude lower than the reflection coefficient, but still much higher than that predicted for a homogenized medium.

These results are not surprising when the resonant nature of air bubbles is taken into account. Indeed, it is well known that bubbles are highly efficient scatterers, even for wavelengths much larger than the bubble size, and this is because bubbles show low-frequency resonances. In particular, the Minnaert resonance is associated with a radially oscillating mode, in which the high compressibility of air with respect to the external medium allows the bubble to expand and contract with a non-negligible amplitude. This phenomenon explains the observed high transmission at low frequency, since radial oscillations of the bubbles radiate sound equally at both sides of the bubble layer. To confirm this idea, the Minnaert resonance of the two-dimensional bubbles used here should occur at a frequency comparable to the ones used in the measurements.

Our calculation for the Minnaert resonance of a two-dimensional bubble is limited to circular bubbles in an infinite fluid medium. When considering a circular bubble of the same area as the rectangular bubbles of our setup, we find a resonance frequency of 157 kHz, which is within the lowest-frequency range studied. This value is to be taken only as an order of magnitude, since a number of approximations are considered in the model, as explained in the following.

First, the exact rectangular cross section of the bubbles was not taken into account. The shape of the bubble is expected to affect the resonance frequency, although to a moderate amount, as demonstrated before [20]. Since in our case the rectangular bubbles have an aspect ratio close to one, we do not expect this effect to be dramatic, but it would add a correction factor on the order of unity.

Second, the model was evaluated for bubbles in a fluid, while in the experiments the bubbles were embedded in an elastomeric medium. It is known that the Minnaert frequency of bubbles in an elastic medium also depends on the shear modulus of the latter, which contributes, together with the gas compressibility, to the restitutive response of the system [12,14]. Considering reasonable values for the PDMS shear modulus in the frequency range used in the experiments, between 0.6 and 1.5 MPa [22,27], and the expression for the Minnaert resonance frequency of a spherical bubble in an elastic medium, this correction is estimated to increase the resonance frequency between 2.5 and 4 times.

Third, for determining the resonance frequency, a single isolated bubble was considered, while in the layer the bubbles were very close to each other. Interactions between bubbles are shown to affect the resonance frequency. On one hand, the presence of multiple bubbles renders the layer a system of coupled oscillators, with as many eigenfrequencies as bubbles. Small differences in size between the bubbles cause the eigenfrequencies, otherwise degenerate, to spread over a range of frequencies [38]. On the other hand, it is also shown that a layer of identical bubbles behaves as an oscillator, the natural frequency of which can be expressed in terms of the resonance frequency of each bubble times a correction factor that accounts for multiple scattering [19]. It is difficult to assess the degree of spread of the resonance-frequency range due to differences in bubble sizes, but, for multiple scattering, we estimate a correction factor of 2 for our experimental parameters.

Finally, all damping mechanisms were neglected in the model. There are three sources of damping: viscous dissipation in the outer medium, thermal losses due to nonadiabatic radial oscillations of the bubble, and radiative damping [33,34]. In experiments, we already normalize by viscous attenuation in PDMS but not for thermal or radiative losses. As for any oscillator, dissipation both slightly increases the resonance frequency and widens the peak of the scattering function around the resonance frequency.

In summary, all of these effects produce correction factors on the order of unity that increase the actual resonance frequency of the bubble layer. A detailed model considering all these neglected elements could be addressed with numerical simulations, but this is beyond the scope of

this work. However, overall, they sustain the possibility of finding appropriate parameters to validate the proposed model and explain the experimental results.

## VI. CONCLUSIONS

We studied the transmission and reflection of sound across a layer of very long rectangular bubbles contained in a polymeric matrix, finding high transmission at low frequencies, which we related to the low-frequency resonance of the bubbles. This Minnaert-like resonance was theoretically determined for a circular two-dimensional bubble in an infinite medium, and the resonance frequency for a single isolated bubble of the same area as the bubbles used in this study was determined to be in the lowest-frequency range studied. Based on this, the bubble array was treated as a homogeneous layer with a resonant-specific acoustic impedance to determine the transmission and reflection coefficients, which showed behavior consistent with the experimental results. Although we could not find direct evidence of this resonance, a minimum of transmission should be detectable by fine-tuning the frequency of the incident wave. These results could be useful for the design and fabrication of absorptive layers.

## APPENDIX A: TRANSMISSION AND REFLECTION COEFFICIENTS ACROSS A HOMOGENEOUS LAYER: CASE OF OBLIQUE INCIDENCE

The transmission and reflection coefficients across a homogeneous layer of thickness $h$ in the case of normal incidence is a classic result that can be found in many textbooks, see, for example, Ref. [28]. The analysis considers incident, reflected, and transmitted pressure waves in the outer medium (of density and sound speed $\rho_{\text{out}}$ and $c_{\text{out}}$, respectively), and two pressure waves inside the layer (of density and sound speed $\rho_{\text{int}}$ and $c_{\text{int}}$, respectively), of amplitudes $A$ and $B$, traveling in the $+x$ and $-x$ directions, respectively. The $x$ coordinate is defined as being

perpendicular to the layer plane. The final expressions are

$$|T|^2 = \frac{1}{1 + 1/4 \sin^2(k_{\text{int}}h)(Z_{\text{int}}/Z_{\text{out}} - Z_{\text{out}}/Z_{\text{int}})^2}, \quad (A1)$$

$$|R|^2 = \frac{1/4 \sin^2(k_{\text{int}}h)(Z_{\text{int}}/Z_{\text{out}} - Z_{\text{out}}/Z_{\text{int}})^2}{1 + 1/4 \sin^2(k_{\text{int}}h)(Z_{\text{int}}/Z_{\text{out}} - Z_{\text{out}}/Z_{\text{int}})^2}, \quad (A2)$$

where $k_{\text{int}}$ is the wave number in the homogeneous layer, and $Z_{\text{out}} = \rho_{\text{out}}c_{\text{out}}$ and $Z_{\text{int}} = \rho_{\text{int}}c_{\text{int}}$ are the specific acoustic impedances of the outer and inner media, respectively (PDMS and air in our case, respectively). Equations (A1) and (A2) predict that transmission is negligible, and the wave is mostly reflected as long as $\sin(k_{\text{int}}h)Z_{\text{max}}/Z_{\text{min}} \gg 1$, where $Z_{\text{max}}$ ($Z_{\text{min}}$) is the maximum (minimum) between $Z_{\text{int}}$ and $Z_{\text{out}}$. Interestingly, if the system satisfies

$$k_{\text{int}}h \ll 1 \quad \text{and} \quad k_{\text{int}}h \, Z_{\text{max}}/Z_{\text{min}} \gg 1, \quad (A3)$$

then most of the acoustic intensity would be reflected and almost nothing transmitted, meaning that a very thin layer (of thickness much lower than the wavelength) would act as a perfect reflector, as long as the ratio of specific acoustic impedances is large enough. This is indeed the case for our measurements with a homogeneous 37-$\mu$m-thick air layer, for which, in the frequency range of TP1, $k_{\text{int}}h \in [0.10, 0.18]$ and $Z_{\text{PDMS}}/Z_{\text{air}} \approx 2338$.

The case of oblique incidence can be treated with the same approach. The incidence angle, $\theta_{\text{in}}$, defined as the angle between the $x$ axis and the incident wave vector, $\vec{k}_{\text{out}}$, is assumed to be known, while the reflected, transmitted, and internal angles, defined analogously, $\theta_R, \theta_T, \theta_A$, and $\theta_B$ are, in principle, unknown. Then, continuity of pressure and normal velocity leads to a linear system that can be solved for the transmission and reflection coefficients, as well as the amplitude of the inner pressure waves, $A$ and $B$. As a necessary condition, one finds directly the relationship between the angles:

$$\theta_R = \theta_T = \theta_{\text{in}}; \quad \theta_A = \theta_B,$$

and Snell's law:

$$c_{\text{int}} \sin\theta_A = c_{\text{out}} \sin\theta_{\text{in}}.$$

The transmission and reflection coefficients in this case are found to be

$$|T|^2 = \frac{1}{1 + 1/4 \sin^2(k_{\text{int}}^x h)(Z_{\text{int}}^x/Z_{\text{out}}^x - Z_{\text{out}}^x/Z_{\text{int}}^x)^2}, \quad (A4)$$

$$|R|^2 = \frac{1/4 \sin^2(k_{\text{int}}^x h)(Z_{\text{int}}^x/Z_{\text{out}}^x - Z_{\text{out}}^x/Z_{\text{int}}^x)^2}{1 + 1/4 \sin^2(k_{\text{int}}^x h)(Z_{\text{int}}^x/Z_{\text{out}}^x - Z_{\text{out}}^x/Z_{\text{int}}^x)^2}. \quad (A5)$$

In these expressions, $k_{\text{int}}^x = k_{\text{int}} \cos\theta_A$ is the component of the internal wave vector perpendicular to the layer, $Z_{\text{out}}^x = Z_{\text{out}}/\cos\theta_{\text{in}}$, and $Z_{\text{int}}^x = Z_{\text{int}}/\cos\theta_A$.

## APPENDIX B: TRANSMISSION AND REFLECTION COEFFICIENTS ACROSS A PERIODICAL GRATING

Here, we summarize the results of the homogenization method, which describes a heterogeneous medium with a spatially varying density and bulk modulus, such as our bubble layer, as an effective medium [29,31]. The effective acoustic properties of the effective medium will depend on the matrix and inclusion densities, $\rho_{\mathrm{out}}$ and $\rho_{\mathrm{int}}$, and bulk moduli, $B_{\mathrm{out}} = \rho_{\mathrm{out}} c_{\mathrm{out}}^2$ and $B_{\mathrm{int}} = \rho_{\mathrm{int}} c_{\mathrm{int}}^2$, as well as the volume fraction of inclusions, $\varphi$. Homogenization yields the effective bulk modulus $B_e$, given by

$$\frac{1}{B_e} = \frac{\varphi}{B_{\mathrm{int}}} + \frac{1-\varphi}{B_{\mathrm{out}}}, \tag{B1}$$

and effective anisotropic mass density:

$$\frac{1}{\rho_e} = \begin{pmatrix} 1/\rho_x & 0 \\ 0 & 1/\rho_y \end{pmatrix}, \tag{B2}$$

where

$$\frac{1}{\rho_x} = \frac{\varphi}{\rho_{\mathrm{int}}} + \frac{1-\varphi}{\rho_{\mathrm{out}}}, \tag{B3}$$

$$\rho_y = \varphi \rho_{\mathrm{int}} + (1-\varphi)\rho_{\mathrm{out}}. \tag{B4}$$

Thus, inside the bubble layer, the sound equation is

$$\nabla \cdot \left( \frac{1}{\rho_e} \nabla p \right) + \frac{\omega^2}{B_e} = 0. \tag{B5}$$

By solving the sound equation in the external and homogenized media, and imposing continuity of pressure and normal velocity, one finds the transmission and reflection coefficients across the effective medium, in a similar way to that for a homogeneous layer:

$$|T|^2 = \frac{1}{1 + 1/4 \sin^2(k_x h)(Z_x/Z_{\mathrm{out}}^x - Z_{\mathrm{out}}^x/Z_x)^2}, \tag{B6}$$

$$|R|^2 = \frac{1/4 \sin^2(k_x h)(Z_x/Z_{\mathrm{out}}^x - Z_{\mathrm{out}}^x/Z_x)^2}{1 + 1/4 \sin^2(k_x h)(Z_x/Z_{\mathrm{out}}^x - Z_{\mathrm{out}}^x/Z_x)^2}. \tag{B7}$$

In these expressions, the component of the internal wave vector perpendicular to the layer is given by $k_x$, and satisfies the dispersion relationship:

$$\frac{k_x^2}{\rho_x} + \frac{k_y^2}{\rho_y} = \frac{\omega^2}{B_e}, \tag{B8}$$

in which $k_y$ is defined by Snell's law, $k_y = k_{\mathrm{out}} \sin\theta_{\mathrm{in}}$. By defining the sound velocities, $c_{x,y} = \omega/k_{x,y}$, the normal specific acoustic impedance of the homogenized

medium is

$$Z_x = \rho_x c_x. \tag{B9}$$

The meaning of $Z_{\mathrm{out}}^x$ is the same as that in Eqs. (A4) and (A5).

---

[1] P. S. Wilson, R. A. Roy, and W. M. Carey, Phase speed and attenuation in bubbly liquids inferred from impedance measurements near the individual bubble resonance frequency, J. Acoust. Soc. Am. **117**, 1895 (2055).

[2] F. Koksel, M. G. Scanlon, and J. H. Page, Ultrasound as a tool to study bubbles in dough and dough mechanical properties: A review, Food Res. Int. **89**, 74 (2016).

[3] H. Medwin, Counting bubbles acoustically: A review, Ultrasonics **15**, 7 (1977).

[4] C. Enrrico, J. Pierre, S. Pezet, Y. Desailly, Z. Lenkei, O. Couture, and M. Tanter, Ultrafast ultrasound localization microscopy for deep super-resolution vascular imaging, Nature **527**, 499 (2015).

[5] M. Kafesaki and E. N. Economou, Interpretation of the band-structure results for elastic and acoustic waves by analogy with the LCAO approach, Phys. Rev. B **52**, 13317 (1995).

[6] M. S. Kushwaha, B. Djafari-Rouhani, and L. Dobrzynski, Sound isolation from cubic arrays of air bubbles in water, Phys. Lett. A **248**, 252 (1998).

[7] M. Kafesaki, R. S. Penciu, and E. N. Economou, Air bubbles in water: A strongly multiple scattering medium for acoustic waves, Phys. Rev. Lett. **84**, 6050 (2000).

[8] M. Minnaert, On musical air-bubbles and the sounds of running water, Philos. Mag. **16**, 235 (1933).

[9] V. Leroy, A. Strybulevych, M. G. Scanlon, and J. H. Page, Sound velocity and attenuation in bubbly gels measured by transmission experiments, J. Acoust. Soc. Am. **123**, 1931 (2008).

[10] V. Leroy, A. Strybulevych, M. G. Scanlon, and J. H. Page, Transmission of ultrasound through a single layer of bubbles, Eur. Phys. J. E **29**, 123 (2009).

[11] V. Leroy, A. Bretagne, M. Fink, H. Willaime, P. Tabeling, and A. Tourin, Design and characterization of bubble phononic crystals, Appl. Phys. Lett. **95**, 171904 (2009).

[12] V. N. Alekseev and S. A. Rybak, Gas bubble oscillations in elastic media, Acoust. Phys. **45**, 535 (1999).

[13] S. Y. Emelianov, M. F. Hamilton, Y. A. Ilinskii, and E. A. Zabolotskaya, Nonlinear dynamics of a gas bubble in an incompressible elastic medium, J. Acoust. Soc. Am. **115**, 581 (2004).

[14] E. A. Zabolotskaya, Y. A. Ilinskii, G. D. Meegan, and M. F. Hamilton, Modifications of the equation for gas bubble dynamics in a soft elastic medium, J. Acoust. Soc. Am. **118**, 2173 (2005).

[15] M. Devaud, T. Hocquet, and V. Leroy, Sound propagation in a monodisperse bubble cloud: From the crystal to the glass, Eur. Phys. J. E **32**, 13 (2010).

[16] V. Leroy, A. Bretagne, M. Lanoy, and A. Tourin, Band gaps in bubble phononic crystals, AIP Adv. **6**, 121604 (2016).

[17] Z. Huang, S. Zhao, M. Su, Q. Yang, Z. Li, Z. Cai, H. Zhao, X. Hu, H. Zhou, F. Li, J. Yang, Y. Wang, and Y. Song, Bioinspired patterned bubbles for broad and low-frequency acoustic blocking, ACS Appl. Mater. Interfaces **12,** 1757 (2020).

[18] V. Leroy, A. Strybulevych, M. Lanoy, F. Lemoult, A. Tourin, and J. H. Page, Superabsorption of acoustic waves with bubble metascreens, Phys. Rev. B **91,** 020301(R) (2015).

[19] M. Lanoy, R.-M. Guillermic, A. Strybulevych, and J. H. Page, Broadband coherent perfect absorption of acoustic waves with bubble metascreens, App. Phys. Lett. **113,** 171907 (2018).

[20] M. Strasberg, The pulsation frequency of nonspherical gas bubbles in liquids, J. Acoust. Soc. Am. **25,** 536 (1953).

[21] H. Ammari, B. Fitzpatrick, D. Gontier, H. Lee, and H. Zhang, Minnaert resonances for acoustic waves in bubbly media, Ann. I. H. Poincaré - AN **35,** 1975 (2018).

[22] I. D. Johnston, D. K. McCluskey, C. K. L. Tan, and M. C. Tracey, Mechanical characterization of bulk Sylgard 184 for microfluidics and microengineering, J. Micromech. Microeng. **24,** 035017 (2014).

[23] D. W. Inglis, A method for reducing pressure-induced deformation in silicone microfluidics, Biomicrofluidics **4,** 026504 (2010).

[24] J. E. Mark, *Polymer Data Handbook* (Oxford University Press, New York, 1999).

[25] A. Folch, *Introduction to BioMEMS* (CRC Press, Boca Raton, 2016).

[26] J. C. McDonald, D. C. Duffy, J. R. Anderson, D. T. Chiu, H. Wu, O. J. A. Schueller, and G. M. Whitesides, Fabrication of microfluidic systems in poly(dimethylsiloxane), Electrophoresis **21,** 27 (2000).

[27] V. Leroy, A. Strybulevych, J. H. Page, and M. G. Scanlon, Influence of positional correlations on the propagation of waves in a complex medium with polydisperse resonant scatterers, Phys. Rev. E **83,** 046605 (2011).

[28] L. E. Kinsler, A. R. Frey, A. B. Coppens, and J. V. Sanders, *Fundamentals of Acoustics* (John Wiley & Sons, New York, 2000).

[29] A. Maurel, S. Félix, and J.-F. Mercier, Enhanced transmission through gratings: Structural and geometrical effects, Phys. Rev. B **88,** 115416 (2013).

[30] C. Qiu, R. Hao, F. Li, S. Xu, and Z. Liu, Broadband transmission enhancement of acoustic waves through a hybrid grating, App. Phys. Lett. **100,** 191908 (2012).

[31] A. Bensoussan, J. L. Lions, and G. Papanicolaou, *Asymptotic Analysis for Periodic Structures. Contributions to Economic Analysis* (North-Holland Publishing Company, Amsterdam, 1978).

[32] M. Devaud, T. Hocquet, J.-C. Bacri, and V. Leroy, The Minnaert bubble: An acoustic approach, Eur. J. Phys. **29,** 1263 (2008).

[33] C. Devin, Survey of thermal, radiation, and viscous damping of pulsating air bubbles in water, J. Acoust. Soc. Am. **31,** 1654 (1959).

[34] A. Prosperetti, Thermal effects and damping mechanisms in the forces radial oscillations of the gas bubbles in liquids, J. Acoust. Soc. Am. **61,** 17 (1977).

[35] V. Leroy, M. Devaud, and J.-C. Bacri, The air bubble: Experiments on an ususual harmonic oscillator, Am. J. Phys. **70,** 1012 (2002).

[36] L. L. Foldy, The multiple scattering of waves, Phys. Rev. **67,** 107 (1945).

[37] V. Leroy, N. Chastrette, M. Thieury, O. Lombard, and A. Tourin, Acoustics of bubble arrays: Role played by the dipole response of bubbles, Fluids **3,** 95 (2018).

[38] V. Leroy, M. Devaud, T. Hocquet, and J.-C. Bacri, The bubble cloud as an *N*-degree of freedom harmonic oscillator, Eur. Phys. J. E **17,** 189 (2005).